Measurement of electron transport in the Madison Symmetric Torus reversed-field pinch (invited)

N. E. Lanier,[a] D. Craig, J. K. Anderson, T. M. Biewer, B. E. Chapman, D. J. Den Hartog, C. B. Forest, and S. C. Prager
Department of Physics, University of Wisconsin–Madison, Madison, Wisconsin 53706

D. L. Brower and Y. Jiang
Department of Electrical Engineering, University of California at Los Angeles, Los Angeles, California 90095-1594

(Presented on 21 June 2000)

A recent study investigating the role of electron density fluctuations in particle transport has been conducted on the Madison Symmetric Torus reversed-field pinch. Four diagnostics enabled this experiment: a high-speed multichord far-infrared laser interferometer, a multichord $H\alpha$ array, a 64-position magnetic coil array, and a Doppler spectrometer that measured impurity ion flow fluctuations. Correlation analysis is used to elucidate the relationship among density, magnetic, and impurity ion flow fluctuations. We observe that the electron density fluctuations are highly coherent with the magnetic fluctuations resulting from core-resonant resistive tearing modes. Moreover, the fluctuation-induced particle transport, obtained from the correlation between electron density and flow fluctuations, indicates that the core-resonant tearing modes do not drive significant particle transport in the plasma edge. We will address these four primary diagnostics, details of the analysis techniques, and principal results from this study.
[DOI: 10.1063/1.1319613]

I. INTRODUCTION

Understanding the link between fluctuations and transport in magnetically confined plasmas remains a significant goal in the pursuit of fusion energy. Recently, a strong experimental push to characterize electron density fluctuations and establish their link to particle transport has been conducted on the Madison Symmetric Torus ($R_0 = 1.5\,\mathrm{m}$, $a = 0.52\,\mathrm{m}$) (Ref. 1) reversed-field pinch.[2] Utilizing the data from four major diagnostics, the relationships among density, magnetic, and radial velocity fluctuations were examined.

This work establishes a strong link core-resonant magnetic fluctuations and fluctuations in electron density. We find the density fluctuations from these modes do not cause significant edge transport and cannot account for measured radial electron flux in the plasma edge. During confinement enhancing inductive current drive experiments, or PPCD,[3,4] we observe a substantial reduction in the density fluctuations associated with the core-resonant resistive tearing modes. Concurrent with this reduction, total electron confinement is improved dramatically in the core. In the following we discuss the critical diagnostics (Sec. II), analysis techniques (Sec. III), and principal results (Secs. IV and V) of this study.

[a]Electronic mail: nlanier@lanl.gov

II. DIAGNOSTICS

Characterization of the electron density fluctuations and investigation of their relevance to particle transport require fluctuation measurements of density, magnetic field, and radial velocity. Furthermore, obtaining the total radial flux profile necessitates the measurement of equilibrium density and ionization source profiles. Here in Sec. II we describe the four principal diagnostics used in this study. We discuss, a far-infrared (FIR) interferometer and $H\alpha$ array, which provide measurements of electron density and source profiles, an ion dynamics spectrometer used for flow fluctuations, and the magnetic pickup coil arrays which measure magnetic field fluctuations.

A. FIR interferometer

Developed in collaboration with the UCLA Plasma Diagnostics group, the FIR interferometer, displayed in Fig. 1, is a vertical viewing, multichord, heterodyne system that is capable of measuring electron density behavior with a high degree of speed and accuracy. The 11 chords view impact parameters ranging from $r/a = -0.62$ to $+0.83$, and are divided into two toroidally separated arrays.

The system functions by using a high-power CO_2 laser to pump twin FIR cavities that produce two semi-independent FIR laser beams.[5] The lengths of the two cavities are adjusted to resonate at slightly different frequencies, so that when mixed produce a modulated signal. The peaks of this modulated signal provide the benchmarks from which a relative phase between chords is measured.

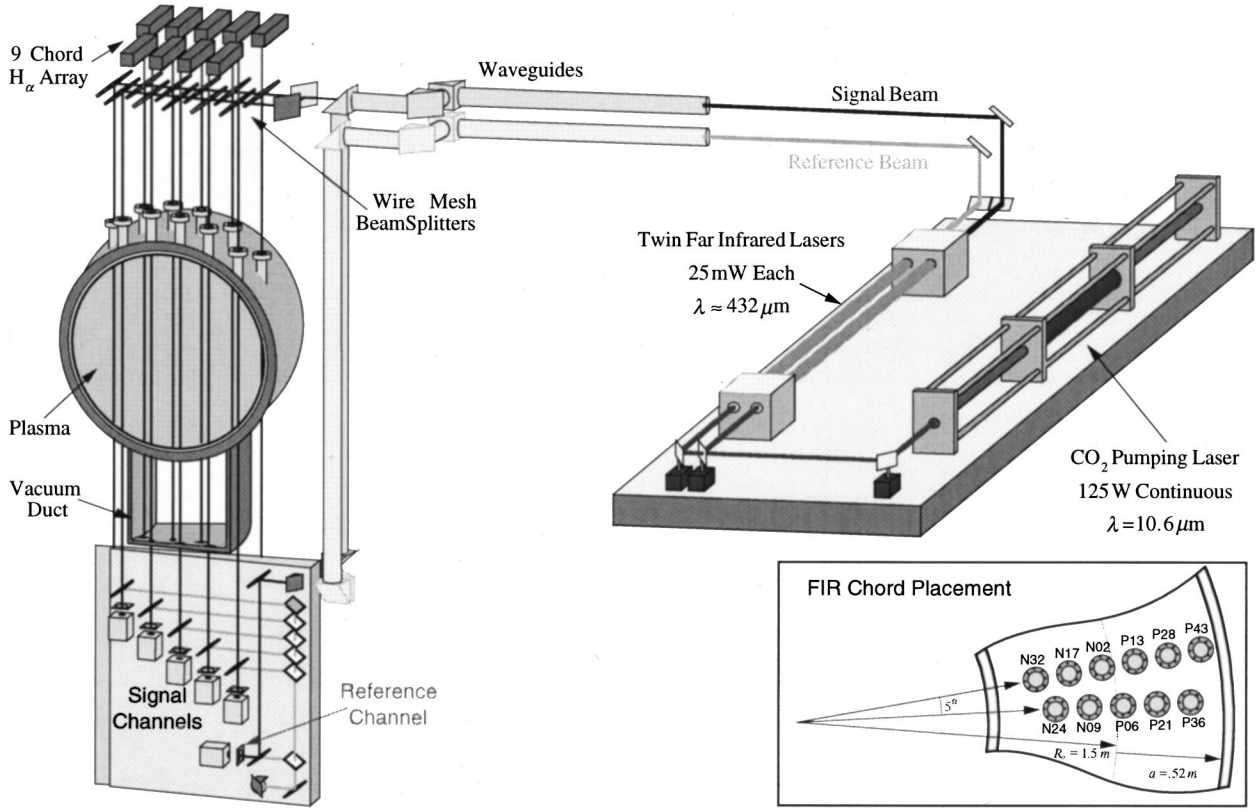

FIG. 1. Far-infrared laser interferometer and $H\alpha$ array.

The interferometer is based on the principle that an electromagnetic wave will propagate through plasma and air at different rates. This difference in propagation can be measured as phase shift (Φ), which will be proportional to the total number of electrons passed as the wave moves through the plasma. This can be written as

$$\Phi(x,t) = \int_{-L/2}^{+L/2} n_e(x,z,t)(z)dz, \tag{1}$$

where n_e is the local electron density, L is the chord length, and x and z are the horizontal and vertical coordinates, respectively. With simulatianeous phase measurements from all 11 chords, the chord-integrated densities are determined and inverted to yield local electron density profiles.

The local density profiles are determined by the MSTFIT equilibrium reconstruction code.[6] The code assumes that the density is a flux function, where flux is calculated by solving the Grad–Shafranov equation with constraints from measured magnetic signals. With spatial flux profiles, coefficients of a set of spline basis functions (density versus psi) are determined from a least squares fit to the data. Errors in the profile are obtained by inverting various perturbations of the raw data in Monte Carlo fashion.

The twin FIR lasers are operated at a wavelength around 432.5 μm, and an interference frequency (IF) of 750 kHz is standard.[7,8] By utilizing a digital phase extraction technique,[9] these parameters yield a frequency response up to 250 kHz and a minimum resolvable phase, measured in vacuum, of 0.03 rad. This phase corresponds to a line-averaged density of $\sim 3.5\times 10^{10}\,\mathrm{cm}^{-3}$ and is about 0.4% of the values measured during plasma discharges.

The frequency response can be doubled by increasing the IF to 875 kHz and the digitization rate to 3.0 MHz. However, there is little gain in operating at higher frequencies since the chord-averaged nature of the measurement serves to severely attenuate the smaller-scale, high-frequency fluctuations.

B. $H\alpha$ and soft x-ray arrays

Knowledge of the neutral hydrogen and low Z impurity excitation rates is vital to determining the electron source rates. The neutral hydrogen ionization rate is extracted from measurements of the $H\alpha$ photon emission. For neutral hydrogen, the ratio of $H\alpha$ excitations to ionizations is about $\sim$0.08–0.09, and remains virtually constant over the range of MST operating conditions.[10]

To measure $H\alpha$ emission profiles, a multichord system was built around nine compact monochromator assemblies. These monochromators, displayed in Fig. 2, take advantage of the dominance of the of $H\alpha$ line by using a narrow bandpass filter to obtain spectral resolution. Each detector is calibrated in place with a calibrating sphere, thus allowing an absolute measure of $H\alpha$ flux to be obtained.

The novelty of this system is its colinear arrangement with the far-infrared interferometer. This configuration averts two key problems. First, since the $H\alpha$ emission is most prominent in the edge, it is extremely sensitive to wall inter-

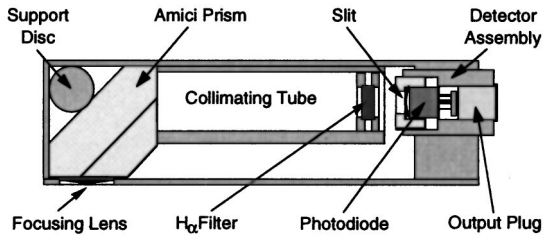

FIG. 2. $H\alpha$ monochromator.

actions. By employing this colinear method, the $H\alpha$ detectors can be focused through the vacuum vessel without viewing any of the interior walls, thereby ensuring that wall contamination is minimized. The second issue is that $H\alpha$ emission can be very asymmetric, both poloidally and toroidally. By simultaneously measuring both $H\alpha$ emission and electron density at the same location, the uncertainties in comparing toroidally displaced measurements are eliminated.

To quantify electron sourcing from low Z impurities, a filtered spectrometer is used.[11] The six channel, multifoil spectrometer is capable of making absolute flux measurements from the high charge states of aluminum, oxygen, and carbon, which are accepted to be the dominant impurities present in MST.[12] From these measured impurity concentrations, electron sourcing via ionization can be constrained.

C. Magnetic coil arrays

The magnetic fluctuations arising from the large-scale core-resonant tearing modes are measured with two extensive arrays of magnetic pickup coils. Each array is composed of coil assemblies that can simultaneously measure the radial, poloidal, and toroidal components of the magnetic field (Fig. 3, inset). The toroidal array is comprised of 64 equally spaced coil assemblies located on the inboard side at 241P, while the poloidal array, located at 180T, uses 16 coil sets (Fig. 3). All the coils are mounted inside the conducting shell, just behind the limiter, and do not interfere with the plasma.

With the dominant poloidal and toroidal mode numbers being $m=1$, $n=5-10$, typical operation of the toroidal array only employs 32 coils, which is sufficient to resolve up to

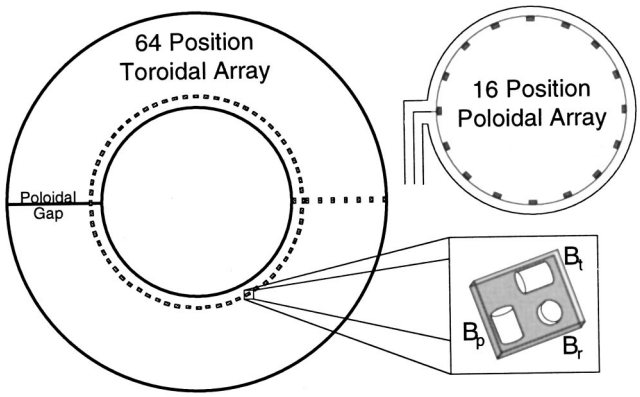

FIG. 3. 64-position toroidal and 16-position poloidal arrays. The inset displays the coil assembly.

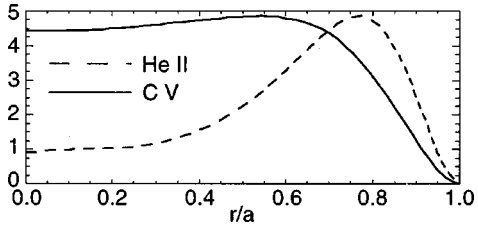

FIG. 4. Impurity profiles of $C-V$ and He II for standard confinement low current plasma discharges.

$n=15$. Moreover, eight coils are used in the poloidal array. In general, the poloidal field ($\tilde{b}_\theta$) pickup coils are preferred over their radial ($\tilde{b}_r$) and toroidal ($\tilde{b}_\phi$) counterparts, since the conducting shell serves to suppress the radial component at the edge, and the purely toroidal field (B_ϕ) prior to plasma startup can be used to calibrate any misorientations that exist in the $\tilde{b}_\theta$ coils.

Fourier decomposition is employed to extract the toroidal harmonics of the magnetic fluctuations from the toroidal array. This is accomplished by defining a time varying cosine, $\tilde{b}_{\theta,n}(t)$, and sine, $\tilde{b}^*_{\theta,n}(t)$, amplitude of the nth toroidal mode as

$$\tilde{b}_{\theta,n}(t) \equiv \frac{2}{N_c}\sum_i \overline{b}_\theta(t)\cos n\phi_i = b_{\theta,n} e^{(m\theta_c+\omega t+\delta_{b_n})}, \quad (2)$$

$$\tilde{b}^*_{\theta,n}(t) \equiv \frac{2}{N_c}\sum_i \overline{b}_\theta(t)\sin n\phi_i = b_{\theta,n} e^{[m\theta_c+\omega t+\delta_{b_n}+(\pi/2)]}. \quad (3)$$

Above we have defined ϕ_i as the toroidal angle of the ith coil and θ_c is the poloidal angle of the array (241°). Once the coefficients $\tilde{b}_\theta(t)$ and $\tilde{b}^*_\theta(t)$ are determined, the mode's amplitude, $A_n(t)=\sqrt{[\tilde{b}_\theta(t)]^2+[\tilde{b}^*_\theta(t)]^2}$, and phase, $\delta_n(t)=\arctan[\tilde{b}^*_\theta(t)/\tilde{b}_\theta(t)]$, are easily computed.

D. Ion dynamics spectrometer

The ion dynamics spectrometer (IDS)[13,14] is a custom designed Czerny–Turner Doppler spectrometer that measures both equilibrium and fluctuating ion flow velocity. Optical light collected from the plasma is channeled, via a fiberoptic bundle, onto a grating which is then dispersed over a 32 channel photomultiplier array. This arrangement offers fast time response (<10 μs), and can be configured to measure toroidal, poloidal, or radial flow components.

Radial velocity fluctuations are measured using a large radial aperture that views a chord passing through the center of the torus. The collection optics were designed to provide equal weighting along the line of sight, and the 4.5 in. port allowed excellent light throughput.

Although a passive chord-averaging diagnostic, radial localization can be enhanced by monitoring the proper choice of impurity. Chosen for their bright emission lines and favorable radial locations, He II and $C-V$ are most commonly employed. Figure 4 displays the density profiles of He II and $C-V$. Monitoring He II, which is most abundant outside $r/a>0.6$, allows excellent measurement of the edge ion

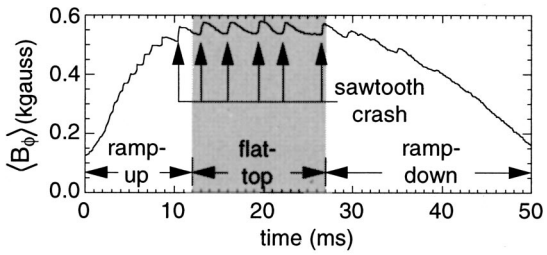

FIG. 5. Average toroidal magnetic field vs time, illustrating the regularity of sawteeth during the flat-top phase of the discharge.

velocity, while $C-V$, which has a broad flat profile inside $r/a<0.8$, is used when measurement of core behavior is desired.

III. ANALYSIS TECHNIQUES

Correlation analysis provided the principal means by which to distill the desired fluctuation information from the wide range of diagnostics discussed above. By correlating the density fluctuations with individual toroidal harmonics of the magnetic fluctuations measured with the 64-position coil array, we are able to extract a toroidal mode number spectrum of the coherent density fluctuations. Correlations between density and radial velocity fluctuations are used to determine the transport implications of $\tilde{n}$. In Secs. III A and III B, we briefly discuss some details of the correlation techniques employed (Sec. III A), and outline the procedure for obtaining local density fluctuation profiles, once a given m and n have been isolated (Sec. III B).

A. Correlation analysis

Correlations among fluctuating quantities are conducted over a large number of realizations. Ensembling over many events provides better isolation of secular behavior because random noise present in the signals averages to zero. When ensembling for the purpose of isolating fluctuation behavior, subtracting the slowly varying equilibrium component becomes very critical. With this in mind, it is important that equilibrium behavior be uniform in all chosen ensembling windows.

A robust feature in standard MST discharges is the presence of large magnetic relaxation events, or sawteeth (Fig. 5). During the flat-top phase of the discharge, sawteeth occur in regular intervals and provide an excellent benchmark for selecting ensembling windows. Typically, the windows are about 4 ms wide and centered at the sawtooth crash time. In high confinement plasmas, where auxiliary current drive has suppressed the sawteeth, ensemble windows are 8 ms wide and start at the PPCD fire time.

B. Density fluctuation profiles

Once the density fluctuation amplitude resulting from a particular toroidal harmonic has been isolated via correlation with the toroidal magnetic array, the radial fluctuation profile can be determined by inverting the amplitudes of the correlated products. For an $m=0$ mode, the inversion proceeds the same as with the equilibrium density, which invokes up–down symmetry. However, if $m\neq 0$, up–down symmetry is violated, and the symmetry of the perturbation must be considered in the inversion process.

In the case where the fluctuation is known to have an $m=1$ structure, we perform the inversion as follows. Let

$$n(r)=n_0(r)+\tilde{n}(r)\cos[\omega t+m\theta+n\phi+\delta(r)], \tag{4}$$

where ϕ and θ are toroidal and poloidal angles, and $\tilde{n}(r)$ and $\delta(r)$ are the radial functions of the amplitude and phase of the density fluctuations, respectively. A chord-integrated measurement of this perturbation can be written as

$$I(x)=I_0(x)+\tilde{I}(x), \tag{5}$$

where

$$\tilde{I}(x)=\int_{-L/2}^{+L/2}\tilde{n}(r)\cos[\omega t+m\theta+n\phi+\delta(r)]dz. \tag{6}$$

Here, x represents the impact parameter of the chord, L is the chord's path length through the plasma, and z is the vertical coordinate. Equation (6) can be simplified to

$$\tilde{I}(x)=\tilde{I}_{\rm amp}(x)\cos[\omega t+n\phi+\Delta(x)], \tag{7}$$

where we have defined

$$\tilde{I}_{\rm amp}(x)\sin[\Delta(x)]=\int_x^a\frac{\tilde{n}(r)\sin[\delta(r)]}{\sqrt{r^2-x^2}}dr \tag{8}$$

and

$$\tilde{I}_{\rm amp}(x)\cos[\Delta(x)]=\int_x^a\frac{\tilde{n}(r)\cos[\delta(r)]}{\sqrt{r^2-x^2}}dr. \tag{9}$$

Equations (8) and (9) can be Abel[15] inverted to arrive at

$$\tilde{n}(r)\sin[\delta(r)]=-\frac{r}{\pi}\int_r^a\frac{d}{dx}\left(\frac{\tilde{I}_{\rm amp}(x)\sin[\Delta(x)]}{2x}\right)\frac{dx}{\sqrt{x^2-r^2}} \tag{10}$$

and

$$\tilde{n}(r)\cos[\delta(r)]=-\frac{r}{\pi}\int_r^a\frac{d}{dx}\left(\frac{\tilde{I}_{\rm amp}(x)\cos[\Delta(x)]}{2x}\right)\frac{dx}{\sqrt{x^2-r^2}}. \tag{11}$$

The parameters $\tilde{I}_{\rm amp}$ and Δ of a specific m and n structure are isolated by correlating the fluctuating part of the integrated density with one Fourier component of the magnetic fluctuations $\langle\tilde{I}\tilde{b}_{m,n}\rangle$. Having obtained the products $\tilde{I}_{\rm amp}\sin(\Delta)$ and $\tilde{I}_{\rm amp}\cos(\Delta)$ for each chord, an Abel inversion is conducted, and the radial functions $\tilde{n}(r)$ and $\delta(r)$ are easily extracted.

IV. RESULTS

Using the data obtained from the diagnostics discussed in Sec. II and the analysis procedures presented in Sec. III, we have characterized the dominant density fluctuations and determined their relevance to edge electron transport. In Secs. IV A–IV C we outline the density fluctuation character

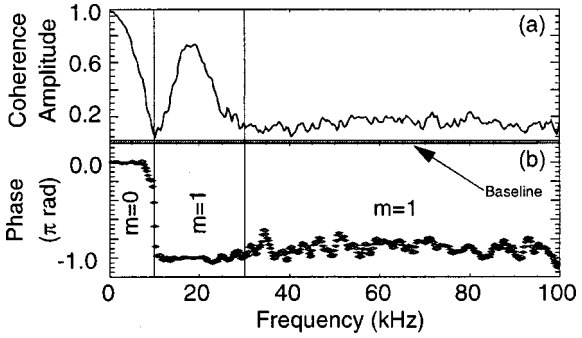

FIG. 6. Coherence (a) amplitude and (b) phase between $r/a=-0.62$ inboard and $r/a=+0.83$ outboard FIR chords. Both chords are at the same toroidal angle.

(Sec. IV A), radial fluctuation profiles (Sec. IV B), and resulting fluctuation-induced radial electron transport (Sec. IV C).

A. Density fluctuation character

Correlation analysis allows the spatial harmonic content of the density fluctuations to be resolved. By correlating between inboard and outboard FIR chords, the m nature can be determined. Figure 6 shows the coherence amplitude and phase between the FIR chords located at $r/a=-0.62$ and $+0.83$. Two highly coherent peaks are evident, one between 10 and 30 kHz, the other below 4 kHz. For the low frequency peak, the chords fluctuate in phase, indicating that the density fluctuations result from changes in the equilibrium or low frequency $m=0$ modes. In the range of 10–30 kHz, the chords fluctuate out of phase and have an $m=odd$ nature. Further correlations with all FIR chords show definitively that this peak has an $m=1$ structure.

The toroidal harmonics of the density fluctuations are determined by correlating the FIR signals with the Fourier decomposed magnetic fluctuations that were obtained from the 64-position pickup coil array. The correlation between chord-integrated density fluctuations and magnetic fluctuations from the core-resonant $m=1$, $n=5-15$ modes is displayed in Fig. 7. In the core, the density fluctuation power is small and poorly coherent with the core-resonant modes [Fig. 7(a)]. As the impact parameter increases, the density fluctuation power increases and a peak develops between 10 and 20 kHz [Fig. 7(b)]. This peak is highly coherent with the core-resonant modes. At the edge, the overall density fluctuation power continues to increase and the peak broadens significantly [Fig. 7(c)]. Although the fluctuation power has increased, the relative coherence to the core-resonant modes has diminished, indicating a greater contribution from small-scale higher frequency fluctuations.

B. Radial fluctuation profiles

As outlined in Sec. III B, the correlated product of the density and magnetic fluctuations can be used to extract the radial fluctuation profiles $[\tilde{n}(r)]$. The density fluctuation profiles for the $m=1$, $n=6-9$ helicities are displayed in Fig. 8 for both standard and PPCD initiated high-confinement discharges.

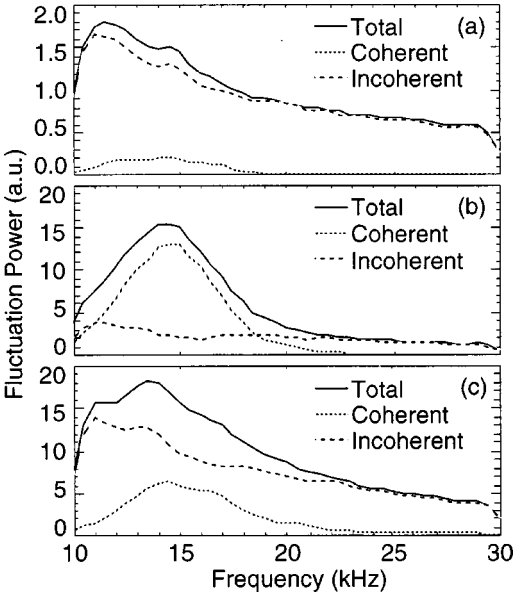

FIG. 7. Total, coherent, and incoherent density fluctuation power for impact parameters of $r/a=$(a)$+0.11$, (b) $+0.54$, and (c) $+0.83$.

In standard discharges, the fluctuation profiles are broad with peak values around 1%–2%. An interesting feature is that, as n increases, the peak in the fluctuation profile moves outward in radius. This is consistent with the expectation that, for a constant density gradient, the density fluctuation from a magnetic tearing mode should be largest near its resonant surface.

During enhanced confinement PPCD discharges, when both the magnetic and chord-integrated density fluctuations are reduced, $\tilde{n}(r)$ drops more than an order of magnitude and

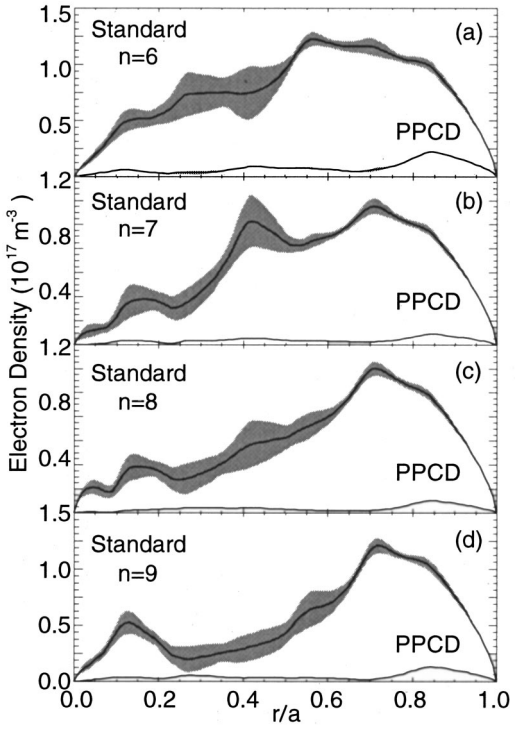

FIG. 8. Radial electron density fluctuation profiles $[\tilde{n}(r)]$ for the $m=1$ $n=$(a) 6, (b) 7, (c) 8, and (d) 9 toroidal components.

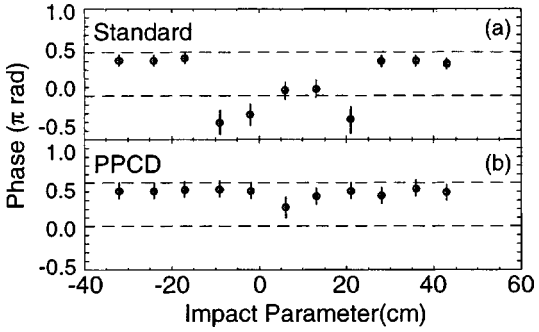

FIG. 9. Radial profile of the phase between the chord-averaged density fluctuations ($\tilde{n}$) and edge radial magnetic field fluctuations for (a) standard and (b) PPCD discharges.

becomes more edge peaked [Figs. 8(a)–8(d)]. Local amplitudes range from ~0.05% in the core to about 0.1% near the edge. The location of the peak is near the toroidal magnetic field reversal surface ($r/a \sim 0.85$) and is independent of the toroidal mode number (n), indicating that the very steep edge density gradient, formed during PPCD, plays a strong role in these fluctuations.

C. Fluctuation-induced electron transport

Information on the fluctuation-induced electron transport is obtained via correlation between the density and radial velocity fluctuations. The fluctuation-induced radial particle flux is

$$\Gamma_r = \langle \tilde{n}\tilde{v}_r \rangle = \gamma |\tilde{n}||\tilde{v}_r| \cos(\delta_{nv}), \tag{12}$$

where γ is the coherence amplitude and δ_{nv} is the phase between $\tilde{n}$ and $\tilde{v}_r$. By investigating the relative phase between the FIR measurements of fluctuating electron density and the radial velocity obtained from the ion dynamics spectrometer, we can assess whether the coherent density fluctuations induced particle transport.

The phase of the correlated product of density and edge radial velocity fluctuations, determined using He II, is displayed in Fig. 9 for standard and PPCD discharges. In both cases, the phase (δ_{nv}) is measured to be $\pi/2$ at the plasma edge. This indicates that the density fluctuations coherent with the core-resonant tearing modes do not cause transport at the plasma edge. This is also consistent with the expectation that such modes do not destroy edge magnetic surfaces.

In the core, the relative phase of the density fluctuations changes during PPCD [Fig. 9(b)]. Because measurements of the core radial velocity fluctuations using $C-V$ were inconclusive, we are unable to make any statement about the local phase between $\tilde{n}$ and $\tilde{v}_r$. However, it is clear that density fluctuations in the core are modified during PPCD.

V. TOTAL ELECTRON TRANSPORT

Concurrent with this change in phase and the reduction of the core density fluctuations, the measured radial particle flux decreases dramatically. In standard discharges, the density profiles are flat in the core, with a steep edge gradient [Fig. 10(a)]. The electron source profile, which is dominated by ionization of neutral hydrogen, appears to be quite broad,

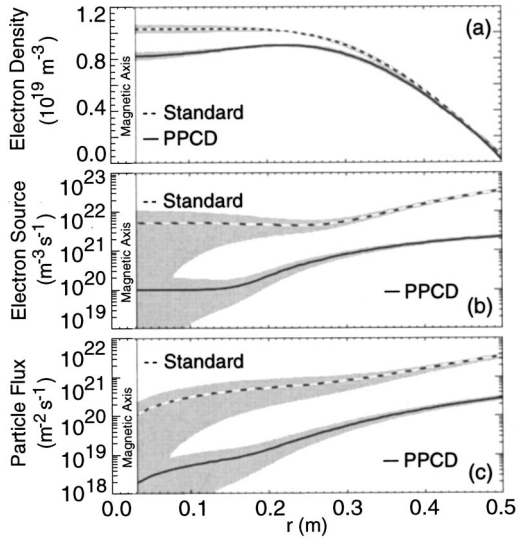

FIG. 10. Radial profiles of (a) electron density, (b) electron source (impurities included), and (c) electron radial particle flux for standard and PPCD discharges.

with substantial sourcing well into the core [Fig. 10(b)]. This leads to a radial particle flux, outlined in Fig. 10(c), that ranges from $\sim 2.0\times10^{20}\,\mathrm{m^{-2}\,s^{-1}}$ in the core, rising to $\sim 3.0\times10^{21}\,\mathrm{m^{-2}\,s^{-1}}$ at the plasma boundary. This edge value is consistent with probe measurements of electrostatic fluctuation-induced particle transport presented by Rempel *et al.* in 1990.[16]

During PPCD discharges, in which initial fueling had been modified such that at peak confinement the density profiles had similar magnitudes, the overall radial particle flux dropped over 10-fold [Fig. 10(c)]. With the decrease in transport reducing the plasma wall interaction, wall recycling drops and electron sourcing from neutral hydrogen falls to immeasurable levels in the core. Furthermore, the density profile broadens and becomes hollow [Fig. 10(a)]. The gradient formation in the core is a clear indicator of confinement improvement.

VI. CONCLUSIONS

By investigating the relationships among data obtained from the far-infrared interferometer, magnetic pickup coil array, and Doppler spectrometer, we have determined that the density fluctuations are highly coherent with the core-resonant resistive tearing modes. Moreover, measurements of the fluctuation-induced particle transport show these fluctuations do not cause significant transport at the RFP edge and result simply from advection of a steep equilibrium density gradient. The magnitudes of the core-resonant radial density fluctuation profiles are about 1%–2% in standard discharges and drop 10-fold during PPCD experiments. Concurrent with this fluctuation reduction, the total radial particle flux drops an order of magnitude.

ACKNOWLEDGMENTS

The authors are especially grateful for the contributions of J. T. Chapman, D. Holly, J. S. Sarff, and the MST group. This work was supported by the U.S. Department of Energy.

[1] R. N. Dexter, D. W. Kerst, T. W. Lovell, S. C. Prager, and J. C. Sprott, Fusion Technol. **19**, 131 (1991).
[2] H. A. B. Bodin and A. A. Newton, Nucl. Fusion **19**, 1255 (1980).
[3] J. S. Sarff, S. A. Hokin, H. Ji, S. C. Prager, and C. R. Sovinec, Phys. Rev. Lett. **72**, 3670 (1994).
[4] J. S. Sarff, N. E. Lanier, S. C. Prager, and M. R. Stoneking, Phys. Rev. Lett. **78**, 62 (1997).
[5] S. R. Burns, W. A. Peebles, D. Holly, and T. Lovell, Rev. Sci. Instrum. **63**, 4993 (1992).
[6] C. B. Forest *et al.*, Bull. Am. Phys. Soc. **42** (1997).
[7] Y. Jiang, N. E. Lanier, and D. L. Brower, Rev. Sci. Instrum. **70**, 703 (1999).
[8] Y. Jiang, D. L. Brower, L. Zeng, and J. Howard, Rev. Sci. Instrum. **68**, 902 (1997).
[9] D. W. Choi, E. J. Powers, R. D. Bengtson, G. Joyce, D. L. Brower, W. A. Peebles, and N. C. Luhmann, Jr., Rev. Sci. Instrum. **57**, 1989 (1986).
[10] L. C. Johnson and E. Hinnov, J. Quant. Spectrosc. Radiat. Transf. **13**, 333 (1973).
[11] N. E. Lanier, Ph.D. dissertation, Department of Physics, University of Wisconsin–Madison, Madison, WI, 1999.
[12] S. Hokin, R. Fonck, and P. Martin, Rev. Sci. Instrum. **63**, 5038 (1992).
[13] D. J. Den Hartog and R. J. Fonck, Rev. Sci. Instrum. **68**, 3238 (1994).
[14] J. T. Chapman and D. J. Den Hartog, Rev. Sci. Instrum. **68**, 285 (1996).
[15] W. M. Barr, J. Opt. Soc. Am. **52**, 885 (1962).
[16] T. D. Rempel, C. W. Spragins, S. C. Prager, S. Assadi, D. J. Den Hartog, and S. Hokin, Phys. Rev. Lett. **67**, 1438 (1991).